Observation of three-dimensional motion of pellet ablatant in LHD

J. S. Mishra[1], R. Sakamoto[2], G. Motojima[2], H. Yamada[2] and LHD experiment group[2]

[1] *The Graduate University for Advanced Studies, Toki, Gifu 509-5292, Japan*

[2] *National Institute for Fusion Science, Toki, Gifu 509-5292, Japan*

1. Introduction

Pellet penetration and particle deposition process study, inside the hot plasma is an absolute interest to achieve the high fueling efficiency. Pellet trajectory deflection in presence of fast ions has been observed in Large Helical Device(LHD), can affect the penetration[1]. In addition LHD has three dimensional magnetic field structure which complicates the pellet plasma interaction and mass deposition process. Therefore it is indispensable to measure the three dimensional pellet ablation, in order to optimize the pellet fueling process and finding of the mechanism behind this in LHD. In this article stereoscopic observation of pellet trajectory deflection in presence of a tangential NBI heated plasma has been discussed.

2. Experimental setup

LHD has major radius, average minor radius and magnetic field strength, 3.9 m, 0.6 m and 2.9 T respectively. The magnetic confinement field is generated by l/m = 2/10 superconducting coils, hence the magnetic field is varies between a vertically elongated and a horizontally helical section throughout toroidal direction. LHD is equipped with a repetitive pellet injector,[2] can inject pellet at 11 Hz repetition rate with a speed of 150 - 550 m/s from the outboard horizontally elongated mid-plane section. Limited port access restricts the number of observation points to obtain three dimensional information about a system. Hence a two point stereoscopic[3] technique is applied to observe the three dimensional pellet motion.

In this technique, a three dimensional spatial point $\mathbf{M} = [\mathrm{X\ Y\ Z}]^T$ is imaged from two or more different locations assuming pinhole camera model as shown in Fig. 1. The respective image point $\mathbf{m} = [u\ v]^T$ for the spatial point can be related as

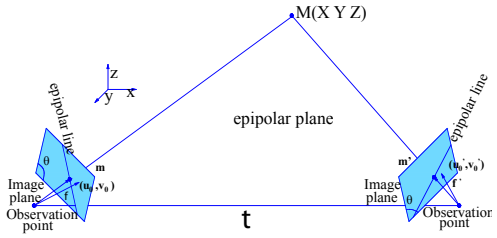

Figure 1: Stereoscopic imaging principle

$$s\tilde{\mathbf{m}} = \mathbf{P}\tilde{\mathbf{M}} \qquad (1)$$

where s is the arbitrary scale factor and $\mathbf{P}$ is the projection matrix of dimension 3×4. This projection matrix is estimated during camera calibration contains the optical and geometrical characteristics of the system. Projection of the three dimensional point $\mathbf{M}$ to two image points gives $s\tilde{\mathbf{m}} = \mathbf{P}\tilde{\mathbf{M}}$ and $s'\tilde{\mathbf{m}}' = \mathbf{P}'\tilde{\mathbf{M}}$. Combining this two expressions the the complete stereoscopic

equation can be written as

$$\begin{bmatrix} P_{14}-uP_{34} \\ P_{24}-vP_{34} \\ P'_{14}-u'P'_{34} \\ P'_{24}-v'P'_{34} \end{bmatrix} = \begin{bmatrix} uP_{31}-P_{11} & uP_{32}-P_{12} & uP_{33}-P_{13} \\ vP_{31}-P_{21} & vP_{32}-P_{22} & vP_{33}-P_{23} \\ u'P'_{31}-P'_{11} & u'P'_{32}-P'_{12} & u'P'_{33}-P'_{13} \\ v'P'_{31}-P'_{21} & v'P'_{32}-P'_{22} & v'P'_{33}-P'_{23} \end{bmatrix} \times \begin{bmatrix} X \\ Y \\ Z \end{bmatrix} \quad (2)$$

The brightest point in one image is assumed to be the the pellet position on that image and the corresponding point on the other image is found by using the epipolar line concept. Therefore knowing the projection matrix and the image coordinates, the spatial position of the pellet can be evaluated.

The pellet injection location with observation points and the direction of tangentially applied NBI beam are shown in Fig. 2. A pair of stereo images from two different locations are taken by using the bifurcated imaging fiber, focused on to the fast camera to maintain the simultaneity of the image. Each bifurcated fiber end has an objective lens of field of view 15°. The fast camera equipped with SR-CMOS sensor has spatial resolution ≈ 90 K pixels and temporal resolution of 50 μs with 2 μs exposure time. The error calculated from the stereo-reconstructed model plane, used for calibration are of 5 mm, 6 mm and 15 mm in X, Y, Z direction respectively.

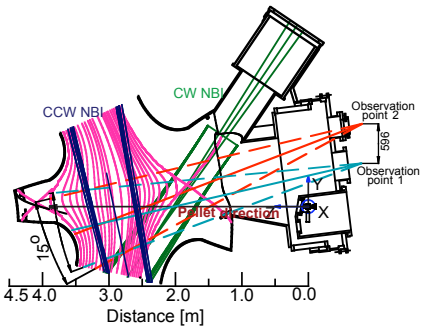

Figure 2: Pellet injection location with observation points and the direction of tangentially applied CW NBI [green] and CCW NBI [blue]

3. Results and Discussions

In this study two types of NBI discharges namely CW NBI of 3.7 MW and CCW NBI of 2.8 MW are taken into consideration. The H_α and the camera intensity signal for an ablating pellet in both NBI conditions are shown in Fig. 3. A bump in H_α and camera signal can be observed [Fig. 3(a)] outside Last closed Flux surface (LCFS) for the CW NBI discharge, however it is absent in case of CCW NBI [Fig. 3 (b)]. This observation is due to the direct heating of the pellet by the CW NBI, as it comes under the influence of NBI path before entering into the plasma [Fig. 2] . A small pedestal in case of CCW NBI indicates the ablation of pellet outside LCFS and is due to the finite plasma in stochastic region of LHD. Pellet trajectory deflection in presence of tangentially applied CW NBI is shown in Fig. 4. The shaded area in the figure indicates the viewing area of the stereo camera. Fig. 4(a) and 4(b) shows the deflection of pellet trajectory along the toroidal plane and poloidal plane respectively. The change in pellet speed along the injection direction (radial: V_R) and perpendicular to it (vertical: V_Z) and (toroidal: V_ϕ) are shown in Fig. 4(c). A similar case for CCW NBI is shown in Fig. 5. Toroidal deflection and poloidal deflection of 20 cm and 10 cm respectively observed in case of CW NBI,

however in case of CCW NBI the toroidal deflection is comparable to former case but the poloidal deflection is negligible. Toroidal deflection velocity (V_ϕ) lies in the range 400 m/s - 800 m/s for CW NBI and 200 m/s - 500 m/s in case of CCW NBI. Toroidal acceleration in case of CW NBI is (0.7 -1.5)$\times 10^6$ ms^{-2} and (0.4 - 0.8)$\times 10^6$ ms^{-2} in other case. The deflection observed is probably due to the asymmetric ablation on both side of pellet by fast ions generated by tangential NBI and subsequently formation of rocket effect in the toroidal direction. Considering one-dimensional heat flux term in the equation of motion along the toroidal direction, pellet acceleration can be calculated in the range (0.15-1.5)$\times 10^6$ ms^{-2},which is in close agreement with the observed acceleration in both cases.

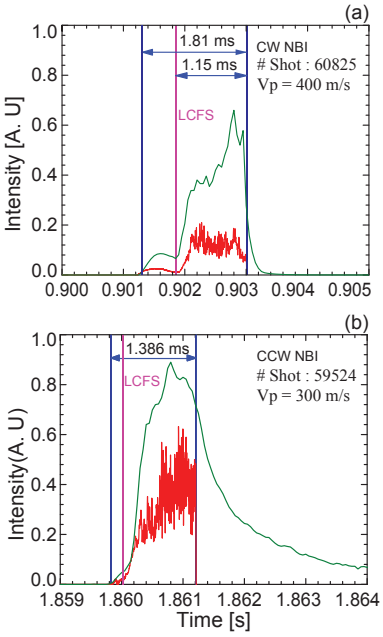

Figure 3: H_α [red] and camera intensity [green] for the ablating pellet in presence of (a) CW NBI and (b) CCW NBI.

Pellet trajectory deflection from its injection direction starts at a normalized minor radius $\rho \approx 0.85$ for CW NBI and $\rho \approx 0.75$ for CCW NBI. This observation can be explained in terms of co-injection and counter-injection. As the toroidal magnetic field is in the CW direction, the CW NBI is co-injection and CCW NBI is counter-injection. The drift orbit of fast ions shifts outward for co-injection and inward for counter-injection[4]. Hence the observation qualitatively agrees with the fast ion deposition profile in LHD. In case of CW NBI injection, pellet speed slowing down along injection direction can be seen in Fig. 4(c) but there is an acceleration of pellet at the last phase of motion [Fig. 5(c)] for CCW NBI injected pellet. The reason behind this is still uncleared and to be investigated.

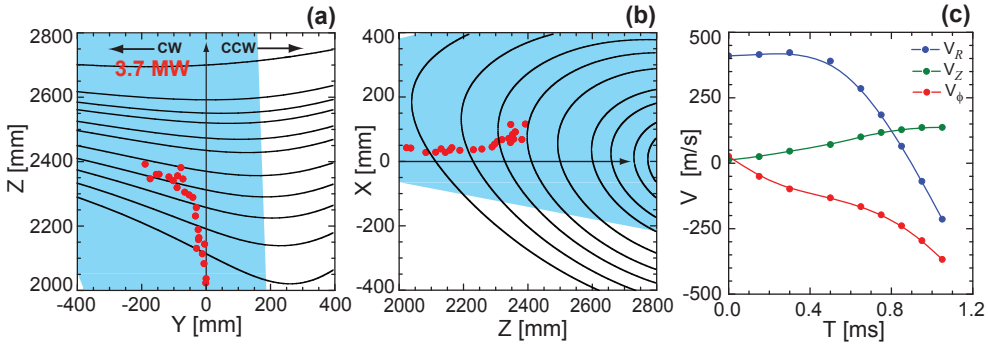

Figure 4: Trajectory deflection along (a) toroidal plane (b) poloidal plane and (c) ablating pellet speed in radial (V_R), vertical (V_Z) and toroidal (V_ϕ) and direction in presence of CW NBI.

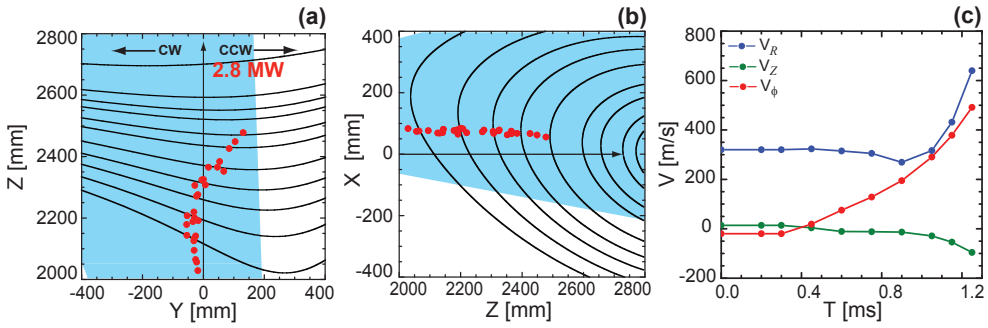

Figure 5: Trajectory deflection along (a) toroidal plane (b) poloidal plane and (c) ablating pellet speed in radial (V_R), vertical (V_Z) and toroidal (V_ϕ) direction in presence of CCW NBI.

Pellet penetration depth considering constant pellet speed along the radial direction with H_α timing compared with the stereoscopic observation in Fig. 6. It can be followed from the figure that observed penetration depth ($\rho \approx 0.75$) is much less than calculated ($\rho \approx 0.63$) value in case of CW NBI and it is more ($\rho \approx 0.65$) than calculated value ($\rho \approx 0.7$) in case of CCW injection. This result is obvious by considering the V_R within pellet life time. Additionally in case of CW NBI pellet deflecting to a squeezing plasma cross section where as the deflection for CCW NBI is to a expanding cross section,which also affects the achievable penetration depth.

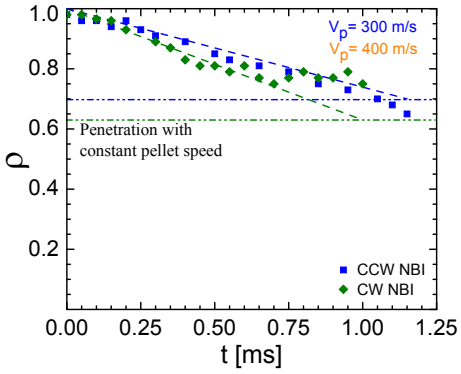

Figure 6: Comparison of pellet penetration depth for CW NBI and CCW NBI. Dash-dot lines indicates penetration depth considering constant pellet speed

4. Conclusion

Three dimensional motion of pellet ablatant analyzed by applying stereoscopic diagnostic. Toroidal deflection of pellet trajectory with acceleration $\approx 10^6$ ms^{-2} observed, with respect to tangential NBI direction. Pellet penetration depth comparison indicates advantage of CCW NBI injection over CW NBI. Reduction of injection speed in case of CW NBI and increase in case of CCW NBI in radial direction is still unclear and to be analyzed further.

References

[1] R. Sakamoto *et al*, Nucl. Fusion 44, 624 (2004)
[2] H. Yamada *et al*, Fusion Engineering and Design 69 (2003)
[3] R. Sakamoto *et al*, Rev. Sci. Instrum 76, 103502 (2005)
[4] S. Morita *et al*, Nucl. Fusion 42, 876 (2002)